

PhyMask: Robust Sensing of Brain Activity and Physiological Signals During Sleep with an All-textile Eye Mask

Soha Rostaminia,¹ S. Zohreh Homayounfar,² Ali Kiaghadi,³ Trisha L. Andrew^{2,4,} Deepak Ganesan,¹*

¹ College of Computer Science, University of Massachusetts Amherst, Amherst MA 01002, USA

² Department of Chemistry, University of Massachusetts Amherst, Amherst MA 01002, USA

³ Department of Electrical Engineering, University of Massachusetts Amherst, Amherst MA 01002, USA

⁴ Department of Chemical Engineering, University of Massachusetts Amherst, Amherst MA 01002, USA

Abstract

Clinical-grade wearable sleep monitoring is a challenging problem since it requires concurrently monitoring brain activity, eye movement, muscle activity, cardio-respiratory features and gross body movements. This requires multiple sensors to be worn at different locations as well as uncomfortable adhesives and discrete electronic components to be placed on the head. As a result, existing wearables either compromise comfort or compromise accuracy in tracking sleep variables. We propose PhyMask, an all-textile sleep monitoring solution that is practical and comfortable for continuous use and that acquires all signals of interest to sleep solely using comfortable textile sensors placed on the head. We show that PhyMask can be used to accurately measure sleep stages and advanced sleep markers such as spindles and k-complexes robustly in the real-world setting. We validate PhyMask against polysomnography and show that it significantly outperforms two commercially-available sleep tracking wearables – Fitbit and Oura Ring.

One Sentence Summary

Sleep phase, microsleep events, physiological metrics and posture are simultaneously recorded using a fabric-based head wrap fit for at-home sleep monitoring

Introduction

There has been a significant commercial interest in measuring sleep given the wide-ranging effects of sleep disruptions, which includes diminished cognitive functioning, diabetes, high blood pressure, heart disease, obesity and depression (1). There is also growing interest in measuring sleep disorders which affects 50 to 70 million Americans of all ages and socioeconomic classes (2). Therefore, it is crucial to scale accurate sleep monitoring such that it can be done less expensively at clinics and more comfortably at home.

But achieving high-quality clinical-grade sleep monitoring with a comfortable wearable device is complicated. That is because sleep is a complex process and monitoring it accurately necessitates many sensors placed at different places on the body. This includes sensors to measure brain activity, eye movement, muscle activity, as well as cardio-respiratory features and gross body movements. To capture these signals, clinical-grade sleep monitoring system (also referred to as polysomnography or PSG) involves electrodes to be placed on the head as well as other locations on the body, which make it highly intrusive. In addition, obtaining a good quality EEG signal requires compromising comfort by using adhesives and attaching electrodes to the skin making it impractical for daily use.

These tradeoffs can be seen across a range of sleep sensing devices in the market (summarized in Figure 1A). There has been significant work on contactless sleep tracking approaches ranging from instrumented bedding to remote tracking via radar or cameras (3–6). While non-contact sensing of sleep is appealing in terms of comfort, they are limited by the fact that they do not contain the single most valuable signal for sleep monitoring i.e., brain electrical activity (Electroencephalography, EEG) as well as eye movement data (Electrooculogram, i.e., EOG). Instead, they primarily rely on surrogate measures such as heart rate, breathing, and body movement signals. While these are useful, they are indirect measures and often highly noisy and sensitive to body orientation and occlusions. As a result, these methods can provide a guesstimate but not precisely measure sleep metrics and fail in various sleep disorder cases. For example, Rapid Eye Movement (REM) sleep stage is known as a state where the person experiences random/rapid movement of the eyes, accompanied with low muscle tone throughout the body, and the tendency to dream vividly. However, the person who is suffering from the REM sleep disorder, usually has violent arm and leg movements during REM sleep stage. These technologies, with the assumption that the body normally freeze and does not move during REM and by solely looking at the cardio-respiratory features and gross body movement, fail to provide accurate measures of sleep where in-home longitudinal sleep tracking is most needed.

There are many wearable devices in the market for sleep sensing, most of which use hard electronic components such as photoplethysmography (PPG) and IMU to measure the pulse wave and body movement on the wrist or fingers (e.g., Fitbit (7), Polar Vivofit (8), Actiwatch (9), Whoop (10), and Oura Ring (11)). In the comfortable textile-based wearables area of research, (12) proposed a novel fabric sensor to monitor pulse wave signal during sleep. In our previous work, Phyjama (13), we also showed that we can measure heart rate and respiration as well as sleep posture through resistive pressure and triboelectric patches sewn into a loosely worn sleepwear. As with the non-contract devices, the main disadvantage of these solutions is lack of ability in monitoring EEG and EOG signals, which is considered critical for high-quality sleep analysis. In the absence of the biopotential signals, these technologies tend to overestimate sleep period, sometimes

by as much as an hour and perform very poorly in estimation of time spent in specific sleep stages (14, 15).

Head-worn solutions are more promising as they allow us to obtain biopotential signals (EEG and EOG) from the head, and several head-worn sleep trackers are commercially available such as Muse (16), Dreem (17), Brainbit (18), and Philips SmartSleep (19). The main drawback of these systems is the rigid structure of the device and the use of hard sensing components that touch the skin on the sensitive head areas. These can make the system highly uncomfortable in different sleep postures and not ideal for continuous long-term sleep tracking. Another debatable aspect of the current head-worn solutions is the quality of the acquired biopotential signals. Majority of these technologies use dry electrodes to avoid adhesives and increase the comfort factor, however, this results in considerable increase in motion artifact (20).

In this work, we present a complete textile-based system for monitoring all the signals for sleep. This builds on a number of our previous efforts on developing individual sensors that provide part of the solution. In the previous work, Chesma (21), we introduced a new thread-based, reusable wet electrode, and showed that this achieves the high signal quality of commercial wet electrodes as well as the comfort and unobtrusiveness of dry electrodes. We presented preliminary results that showed that these electrodes were viable for measuring eye movement patterns. We also presented a fabric-based piezoionic pressure sensor (22) and showed that this is sensitive to pulse signals that can be obtained when the sensor is placed over the supraorbital artery of a user. These sensors, however, provide an incomplete measure of sleep. For example, the lack of EEG results in low accuracy in measuring sleep stages particularly for individuals with sleep disorders, and a pressure sensor on a single position on the head can be highly unreliable in natural settings since the signal quality can vary across individuals and sleep postures. Thus, there is a need for a holistic multi-modal solution that can provide reliable and robust measures of sleep in a natural setting.

In this work, we bridge this gap and develop a complete multi-modal sleep sensing system that is designed using comfortable textile-based sensors, and that is robust to variability in natural settings. We show that a single head-worn device that leverages solely textile-based sensors can provide nearly all the parameters that are used in clinical-grade sleep monitoring including accurate estimates of head-based measures (EEG and EOG), physiological parameters (respiratory and cardiac rhythm) and gross body movement from the head.

Our work makes notable contributions towards a practical daily-use system that is comfortable yet accurate. We show for the first time that a fabric-based electrode can be used to accurately measure the EEG micro-events during sleep such as spindles and k-complexes. This is important since their characteristics, e.g., frequency of their occurrence, can unveil a great amount of information regarding the cognitive state of the mind (23). For example, the density of spindles has been shown to be associated with memory consolidation during learning (24) and cerebrospinal fluid biomarkers of Alzheimer's disease (25) and K-complexes are almost invariably present at the start of seizures (26). We also validate our sensors signal quality in a more realistic setting for continuous long-term sleep tracking.

A novel feature of our work is that we are also able to sense physiological signals (respiratory and cardiac rhythm) and gross body movement from the head without requiring any additional devices. These signals are often considered key auxiliary signals to measure for sleep tracking and sleep disorders such as apnea and periodic limb

movement (27). We propose a novel configuration of pressure sensors to not only measure the cardio-respiratory features in natural settings and different sleep postures, but also to track sleep posture and gross body movement.

We design and fabricate a fully functioning prototype of a comfortable all-textile sleep tracking device (shown in Figure 1B) that includes the fabric-based sensing elements, fabric-based wires, low-power circuit for signal amplification and data acquisition, a wireless radio for data transfer, and tailored algorithms for physiological signals and sleep micro-events tracking.

We perform exhaustive data collection studies to validate our device and compare it against PSG ground truth and two other wearable sleep trackers such as Fitbit wristband and Oura Ring. We show that PhyMask is able to accurately detect sleep stages with an F1 score of 0.91, and greatly outperforms Fitbit (F1 score of 0.64) and Oura Ring (F1 score of 0.7).

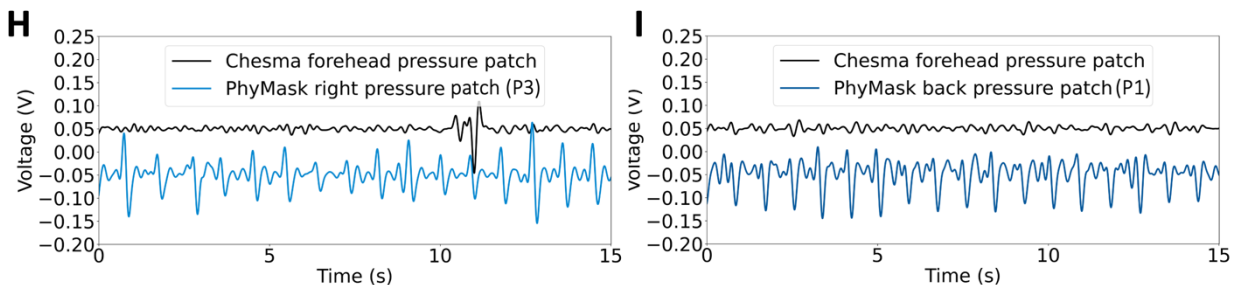
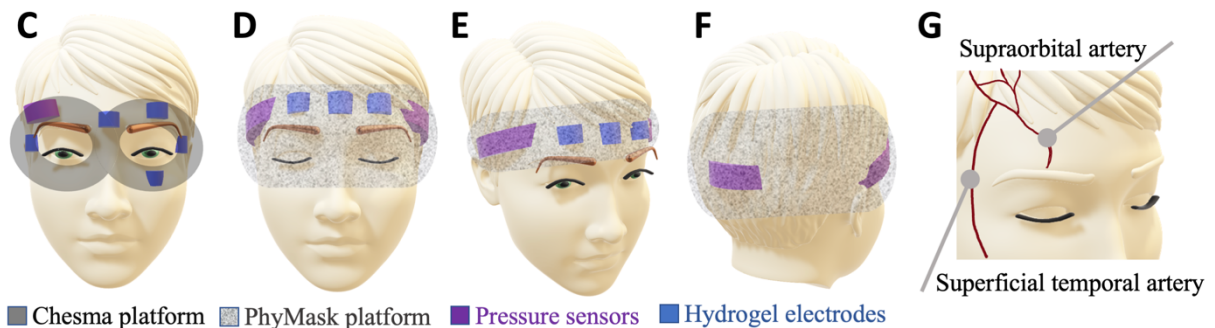
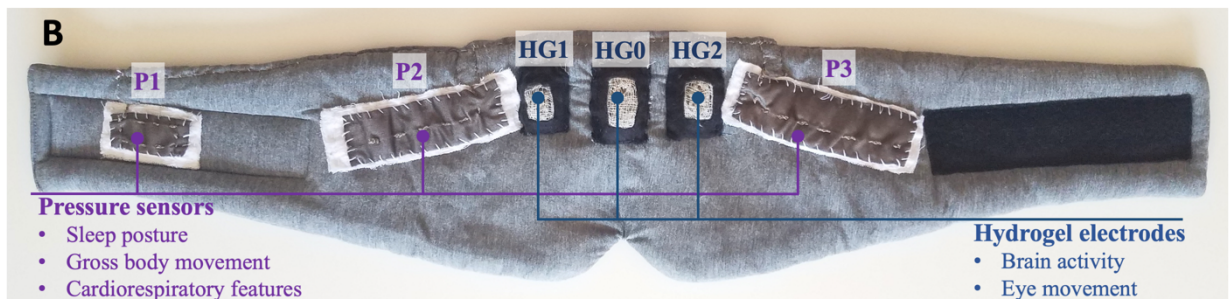
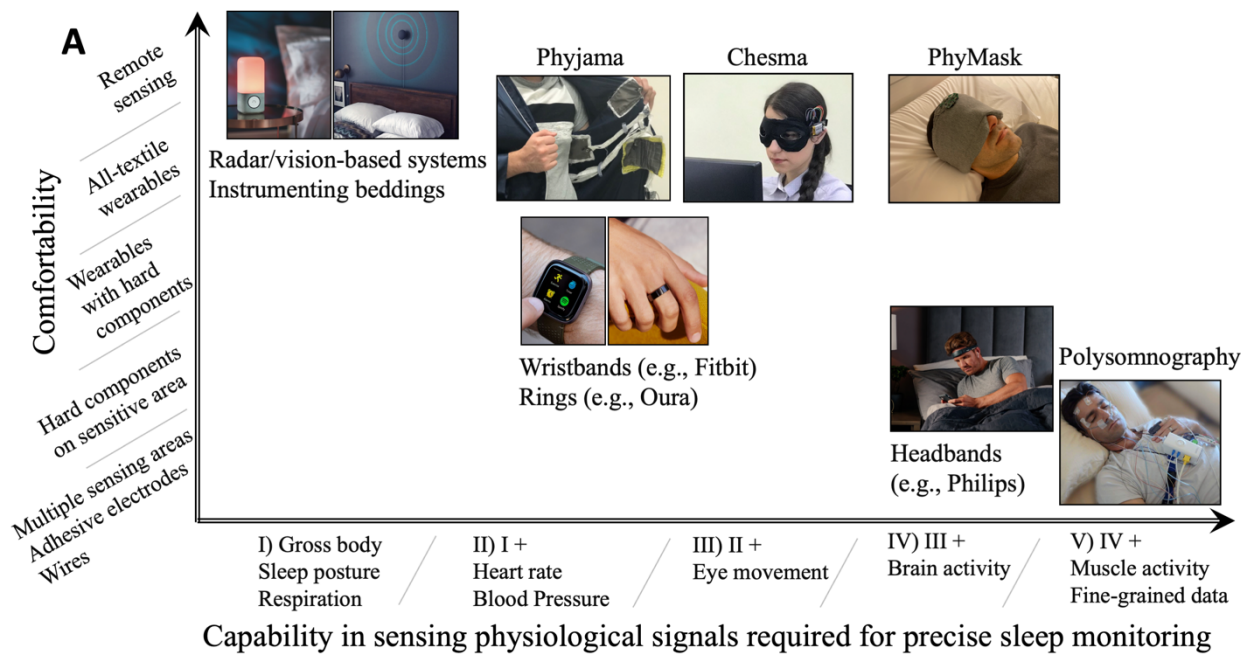


Fig. 1. Summary of current sleep tracking solutions, image of PhyMask, schematic drawings of electrodes placement, and comparison of Chesma and PhyMask. (A) Comparing existing sleep monitoring solutions in terms of comfort and capability in sensing various signals. **(B)** Image of PhyMask platform. **(C)** Schematic drawing of Chesma’s sensors placements. **(D)** Front, **(E)** side, and **(F)** rear views of PhyMask’s sensors placements. **(G)** Schematic drawings of supraorbital and superficial temporal arteries. **(H)** Comparing pulse signal of Chesma and PhyMask platforms, when the user is lying on their right. **(I)** Comparing pulse signal of Chesma and PhyMask platforms, when the user is lying on their back.

Results

Comfortable and robust sleep mask design

While it is possible to obtain sleep markers using a combination of devices, say one on the head for EEG and EOG (16, 19), and another on the body for cardio-respiratory rhythm and movement (11, 13), it is more ideal to obtain all metrics from a single device on the head. Since the head area is sensitive, we remove all hard sensing components from the head-worn device and rely solely on textile-based and soft sensing elements that can be embedded in a sleep mask. Such a design can eliminate rigid sensing elements from being in direct contact with the skin on the head area. While eliminating the hard sensing elements does not preclude need for other rigid electronic components like the microcontroller, radio and battery, these are easier to place in a more conducive location compared to the sensor which needs to be in contact with the skin. We can also route signals from textile sensors through textile-based conductive threads to a microcontroller platform and batteries that are placed away from the head, for example, on the arm. This can allow us to dramatically change how we view comfort for head-worn sensing elements.

Given such an all-textile head-based sensing device with fabric-based sensors, we describe how we optimize the layout of sensors and how we obtain the whole range of sleep markers outlined above from only the head without requiring additional sensors while being robust under different sleep postures and in the presence of inevitable movements that will occur during sleep.

Robust sensing of biopotential signals with textile electrodes. As discussed earlier, in order to extract biopotential signals such as EEG and EOG, we are looking for a fabric-based electrode that is comfortable, robust, and provide reliable high signal-to-noise ratios (SNRs). Hence, we leverage fabric-based, reusable wet electrode that is constructed using the technology that we proposed in the prior work (21). These electrodes have a layer of composite hydrogel, which when hydrated, mechanically behaves like the foams used in the standard electrodes. This is sufficiently cushion-like to minimize motion artifacts in the absence of any harsh skin adhesives. The advantage of these electrodes is that they overcome the aesthetic drawback of requiring adhesives to have contact with the skin while simultaneously providing strong signal integrity. In addition, they address the lack of reusability of the commercial wet electrodes.

EEG and EOG are both biopotential signals and can be captured with the same set of electrodes. In order to reduce the computational cost of the system, we need to choose the minimum number of electrodes that can be embedded into a sleep mask and provide reliable EEG and EOG signals concurrently. In (21), our focus was to capture precise horizontal and vertical eye movement patterns, therefore, as illustrated in Figure 1C, the conventional EOG electrodes placement was chosen. However, for the purpose of sleep tracking, the general knowledge of the eye movement patterns suffices, and we potentially can reduce the number of electrodes. On the other hand, in order to be able to capture strong EEG signals, the electrodes should be placed closer to the brain area. Thus, we place one electrode on top of each left and right eyes (HG1 and HG2, respectively) and one in the middle (HG0), serving as both reference and common ground (shown in Figure 1D and E). HG1 and HG2 electrodes are respectively closest to the Fp1 and Fp2 sites according to the standard 10-20 EEG recording guideline (28) and can conveniently capture horizontal EOG signal which is sufficient for the purpose of sleep stage tracking.

Robust fabric-based physiological signals sensing on the head. Now the question is how to obtain robust physiological signals such as pulse and breathing, as well as gross motor activity on the head using comfortable textile-based sensing elements. In (21), we showed that our proposed sensitive fabric-based pressure sensor is effective in capturing the pulse signal at the supraorbital artery position on a single user (the sensor placement is shown in Figure 1C). While this is promising, such a sensor placement cannot robustly provide the heartbeats in different sleep postures. Two examples are illustrated in Figure 1 (H and I), where the participant is lying on their right and back, respectively, and the pressed pressure patch provides reliable pulse signal, while the patch in the supraorbital position fails in providing robust signal. In this work, we leverage the pressure sensors that are constructed using the technology that was proposed by prior work (21), however, we carefully study and optimize the sensors count and placement so that they can provide reliable and robust signals for various users and in different sleep posture settings (the results are summarized in Figure 3).

For cardiac sensing, we leverage the key observation that the cyclical movement of blood from the heart to the head via the abdominal aorta and the carotid arteries causes the head to move imperceptibly in a periodic manner. Similar oscillations can also be observed during respiration since each inhale and exhale action results in body movements (29). Therefore, unlike the previous work, where we only sense the artery pulse on the forehead, we leverage fabric-based pressure sensors to measure both the pressure exerted by blood pulsing through the facial artery as well as the small subtle head vibrations caused by blood pumping and respiration. In order to make the system robust in various sleep postures, we place the pressure patches on the back (P1), left (P2), and right (P3) of the sleep mask, where at least one of the patches is pressed on the pillow under the user's head weight in different sleep postures (shown in Figure 1D-F). For precise placement of the pressure sensors and in order to achieve the maximum heart rate sensing ability, we look more closely at the physiology of the head. Figure 1G illustrates the anatomy of the arteries passing through the head. The superficial temporal artery is a major artery of the head. It arises from the external carotid artery when it splits into the superficial temporal artery and maxillary artery. Its pulse can be felt above the zygomatic arch, above and in front of the tragus of the ear. Therefore, P2 and P3 sensors are made bigger and placed slightly tilted ($\sim 15^\circ$) on the temple area, allowing for the pulse waveform from the frontal branch of superficial temporal artery to be measured. This layout of the sensors also enables detecting the head posture on the pillow and can capture the pressure changes caused by gross body movement.

Longitudinal EEG signal measurement with fabric-based electrodes during sleep

In this section, we explore our electrode's ability in measuring brain wave signals during a longitudinal sleep study. To the best of our knowledge, this is the first time to measure electroencephalogram (EEG) with all-fabric sensing elements during sleep. The validation of this sensor can potentially impact the next generation of EEG monitoring wearable devices.

We evaluate the EEG signal quality using the coherence measure. This metric is known to identify the level of coupling in cortical pathways given its sensitivity to signal phase difference. Maximum coherence occurs when the phase difference is fixed between two signals and a near zero coherence value indicates a random phase difference between signals over time (30, 31). Coherence is calculated as

$$C_{xy}(f) = \frac{|G_{xy}(f)|^2}{G_{xx}(f)G_{yy}(f)} \quad (1)$$

where $G_{xy}(f)$ is the Cross-spectral density between x and y , and $G_{xx}(f)$ is the autospectral density of x .

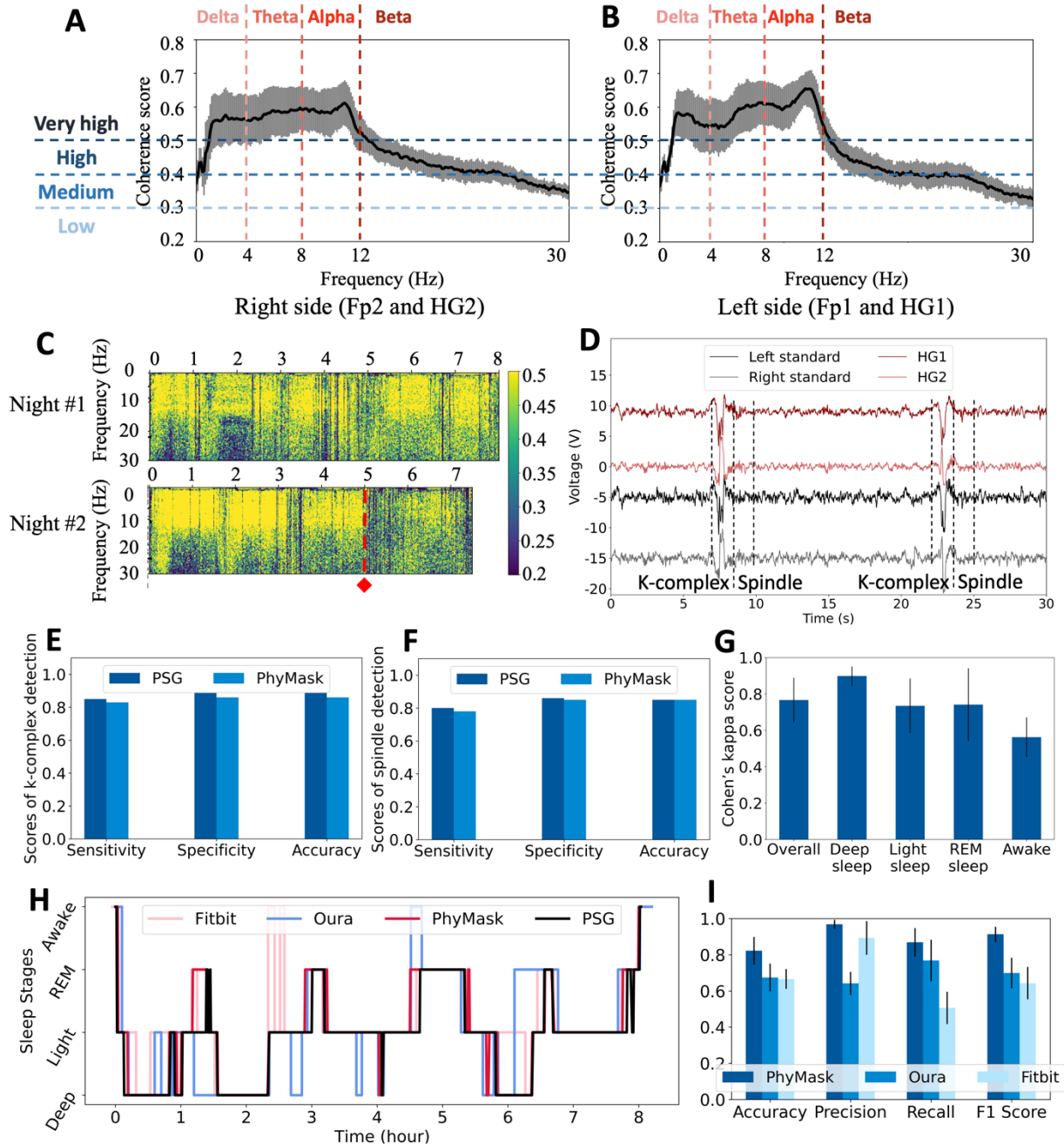


Fig. 2. Analysis of PhyMask EEG signal quality, PhyMask results of sleep stages and micro-sleep events detection, and PhyMask comparison against Oura and Fitbit. (A) and (B) illustrate the averaged coherence measures over each frequency domain across all nights for HG2/Fp2 and HG1/Fp1 groups of signals, respectively. (C) Time series of the coherence score of the HG2/Fp2 pair for two different nights. While the coherence is consistently high for night #1, for night #2, it degrades after 5:00 due to sudden body motions. (D) EEG signals captured from HG1 and HG2 electrodes along with the ground truth signals captured from standard wet electrodes. Two sets of k-complex followed by a spindle are presented at time 8s and 23s. (E) Comparing k-complex detection of PhyMask versus PSG. (F) Comparing spindle detection of PhyMask versus PSG. (G) Median Cohen's kappa score of PhyMask in sleep stage classification over all five

sleep sessions. **(H)** The extracted sleep stages of one night for ground-truth (PSG), PhyMask, Oura, and Fitbit. **(I)** Comparing accuracy, precision, recall, and F1 score of PhyMask, Oura, and Fitbit in sleep stage tracking over all five sleep sessions.

The goal is to evaluate how precise our electrodes can pick up the brain signals with respect to the gold standard EEG recording approach used in PSG, in an uncontrolled and naturalistic setting over a long time of wear. For this, we asked a participant (Male, weight = 160lbs) to wear PhyMask and PSG EEG recording cap for five nights during sleep and we collected the signals for a total of 2118 minutes (~ 7 hours per night). The details of this experiment can be found in Study design section. In order to evaluate the coupling between the PhyMask EEG recording and the ground truth PSG EEG recording, we calculate the coherence for HG1 and HG2 PhyMask electrodes with respect to their closest PSG electrodes, which are Fp1 and Fp2, respectively. Coherence is calculated over 30-second epochs. The calculated coherence values for all epochs are then averaged over all five nights of recording.

Figure 2A and B illustrate the averaged coherence measures over each frequency domain across all nights. As suggested by previous studies in EEG signal analysis (31), we label the coherence scores as following: low (0.2 to 0.3), medium (0.3 to 0.4), high (0.4 to 0.5), and very high (0.5 to 1). As it can be seen, the majority of frequency domains have very high coherence scores, confirming the maximum coupling between our fabric-based hydrogel electrodes and the standard gold-cup electrodes. Please note that for analysis of EEG signal during sleep, we are more interested in the Delta (0.5 to 4 Hz), Theta (4 to 7 Hz), and Alpha (8 to 12 Hz) sub-bands, as the Beta (12 to 25 Hz) is present when the person is awake with open eyes and is actively thinking (31).

While Figure 2 (A and B) illustrates very high coherence for the two groups of signals, it is also important to understand whether the coupling changes as time progresses. In order to investigate this factor, we have plotted the coherence score of the HG2/Fp2 pair for two different full-night sleep sessions in Figure 2C. For night #1, the consistently high coherence score (above 0.4) in lower frequency band (0.5 to 12 Hz), which includes Delta, Theta, and Alpha waves, indicates good performance and high coupling between HG2 electrode and standard Fp2 electrode. However, for night #2, the coherence degrades after time 5:00 (marked with a red arrow). The reason for this observation is that during that time period, the user had sudden body movements and roll-overs that resulted in PhyMask's displacement (about 3cm shift to the right). We see that even with this level of displacement, the average coherence measure is around 0.4 which is well within the acceptable range (31).

Sleep spindle and k-complex detection

As discussed earlier, one of the main advantages of acquiring the EEG signal during sleep is that we can detect and analyze the sleep micro-events such as spindle and k-complex. In this section, we evaluate 1) how well PhyMask is able to detect spindles and k-complexes, and 2) how PhyMask compares to PSG-based spindle and k-complex detection; PSG has higher-dimension EEG signals captured by standard electrodes from various points on the scalp, so it provides a measure of the best-case performance.

In order to compare the performance of PhyMask with PSG in sleep micro-event detection, spindle and k-complex events have been annotated in both PhyMask and PSG sleep data separately. The details of the ground truth labeling procedure can be found in

Study design section. Figure 2D illustrates an example of spindle and k-complex events captured from both systems.

We build a classifier for sleep micro-event detection and train it separately on PhyMask EEG data and the gold standard PSG. The details of signal processing and classifier algorithm are explained in PhyMask processing pipeline section. The results of running the two sets of classifiers using K-fold ($k = 20$) cross validation is summarized in Figure 2 (E and F). Due to the highly imbalanced nature of the data, we use sensitivity and specificity (Equation S1) measures for evaluating the performance of the micro-event detectors as also common in the literature (32, 33).

Our results are very promising and show that: (1) PhyMask accurately detects spindle and k-complex events with higher than 0.8 sensitivity, specificity, and accuracy scores, and (2) PhyMask performs as precise as PSG in spindle and k-complex detection. This means that PhyMask is capable of recording high fidelity EEG signals that contain the micro-sleep events such as spindles and K-complexes.

Validation of PhyMask against polysomnography for sleep stage tracking

In this section, we evaluate the quality of the PhyMask signal against gold-standard PSG for the purpose of sleep stage tracking. In order to do this, both PhyMask and PSG sleep data (more than 35 hours of sleep data) have been annotated by sleep experts into five sleep stages, i.e., N1, N2, N3 (Deep sleep), REM, and Awake. Due to the low number of N1 stage instances in our dataset, we grouped both N1 and N2 stages as Light sleep. In order to quantify the level of agreement for annotated sleep stages between PhyMask and PSG, we use Cohen's kappa defined as follows:

$$\kappa = \frac{p_o - p_e}{1 - p_e} \quad (2)$$

where p_o is the relative observed agreement among raters, and p_e is the hypothetical probability of chance agreement, using the observed data to calculate the probabilities of each observer randomly seeing each category. If the raters are in complete agreement, then $\kappa = 1$. If there is no agreement among the raters, $\kappa = 0$. It is possible for the statistic to be negative, which implies that there is no effective agreement between the two raters, or the agreement is worse than random.

It is well-known that there exists inevitable variability and disagreements between human experts on epoch ratings – Wang et al. found kappas of 0.72-0.85 between two human raters and kappas of 0.82–0.85 between well-performing raters. Therefore, a Cohen's kappa of 0.8 is considered to show strong agreement once we take into account such variabilities. Figure 2G summarizes, for each sleep stage, the Cohen's kappa coefficients over all five sleep sessions (total number of epochs = 4236). The overall performance of PhyMask reaches the state of the art with a median Cohen's kappa of 0.77. For most of the sleep stages, PhyMask agrees very well with the PSG. This high level of agreement between PhyMask and PSG further validates the quality of the measured EEG signal and shows that PhyMask successfully captures information that is critical for sleep stage tracking.

The common misclassified stage in PhyMask data is Awake. In order to better understand when sleep stage misclassifications happen, we calculate the confusion matrix (Figure

S1A), where each data point in the confusion matrix represents a 30-second epoch. As can be seen, the awake stage is mostly confused with the REM stage. Since, these stages have overlapping frequency bands (13Hz-30Hz), the main distinguishing signal between the two is the EOG. During the REM stage, as its name suggests, fast rapid eye movements occur as opposed to slow rolling eye patterns that happen during the Awake/drowsiness stage. PhyMask can only capture the horizontal eye movements; however, human raters are trained on conventional data that includes both horizontal and vertical eye movement patterns. We believe that this might have led to lower classification accuracy in this case, and we hypothesize that in the future, training a classifier on the PhyMask data should significantly help with this.

Comparison between PhyMask and commercial sleep trackers

In this section we compare PhyMask with two other commercially-available sleep tracking devices i.e. Fitbit Charge 2 and Oura Ring. Figure 2H illustrates the extracted sleep stages during the same night from the three devices compared to the PSG ground-truth system. The results of the remaining four nights can be found in Figure S2.

Figure 2I summarizes the results of PhyMask, Oura, and Fitbit in detecting all of the sleep stages over all nights data. PhyMask outperforms the other two devices in terms of all four metrics (accuracy, precision, recall, and F1 score defined in Equation S2), which demonstrates the advantage that PhyMask offers in accurate sleep stage tracking by leveraging its capability in recording the EEG signal.

We also calculate the Cohen's kappa measures and confusion matrices for Oura and Fitbit (Figure S1 (B and C)). Oura (median kappa = 0.54) and Fitbit (median kappa = 0.51) have much lower kappas than PhyMask (median kappa = 0.77). Low accuracy of these sleep trackers in detecting sleep stages has also been observed by previous studies (34, 35). Since we do not have access to the raw data captured by Oura and Fitbit sleep tracking algorithms, we cannot fully analyze their behaviour. However, if we look at the confusion matrices, we find that Oura has a very low recall for the Awake stage. This is because Oura does not provide the micro-awake events after sleep onset in their provided sleep hypnogram on the dashboard. They instead seem to be reported as the closest sleep stage and that is why the predicted labels for Awake events by Oura are distributed almost evenly among all the stages. Fitbit, on the other hand, has a noticeable bias towards classifying sleep sessions as the Light sleep stage. Figure S1C shows that nearly half of the Deep sleep stage epochs are wrongly classified as Light stage. This is an example where leveraging the EEG signal can greatly boost the performance as these two stages can easily be differentiated based on their frequency content (Deep: 0.5-4 Hz and Light: 4-8 Hz).

Head posture and gross body movement estimation

The head posture information during sleep can be useful in understanding which posture leads to better or worse sleep quality. For example, lying on the back is usually not recommended for sleep apnea patients (36). Figure 3A shows the baseline signal for the P1, P2, and P3 pressure patches when a user is lying in different sleep postures for a total of 15 minutes. As it can be seen, in each sleep posture, the pressed patch has the lowest baseline. This is aligned with our expectation as the voltage being measured via the voltage divider circuit (explained in PhyMask board design section) is inversely

proportional to the pressure, so lower voltage means higher pressure. We find that a simple decision tree can easily identify posture with 100% accuracy across all subjects.

PhyMask is also able to capture the gross body movement. In order to evaluate this, we asked our participants to mimic both smooth and jerky limb movements that are common during sleep in each sleep posture. An example signal is shown in Figure 3B, when the user is lying on their back and moving their hand. It can be seen that the pressure signals voltage, especially for the pressed patch, changes dramatically. Please note that the small periodic spikes on the signals correspond to the heartbeats.

The median variance of baseline signal voltage of the three patches for stationary, hand movement, and leg movement scenarios across all sleep postures and over 10 participants are illustrated in Figure S3. As can be seen, the variance difference between the limb movement scenarios and the stationary scenario is very distinct. We can also see that the signal corresponding to the hand movement scenario has lower variance compared to the leg movement scenario since people in general use more force to move their legs as opposed to their hands due to the legs physical characteristics such as weight and length which results in applying more pressure on the patches. As a result, even naive thresholding on the variance of the pressure patch signals can identify different types of gross body movement events.

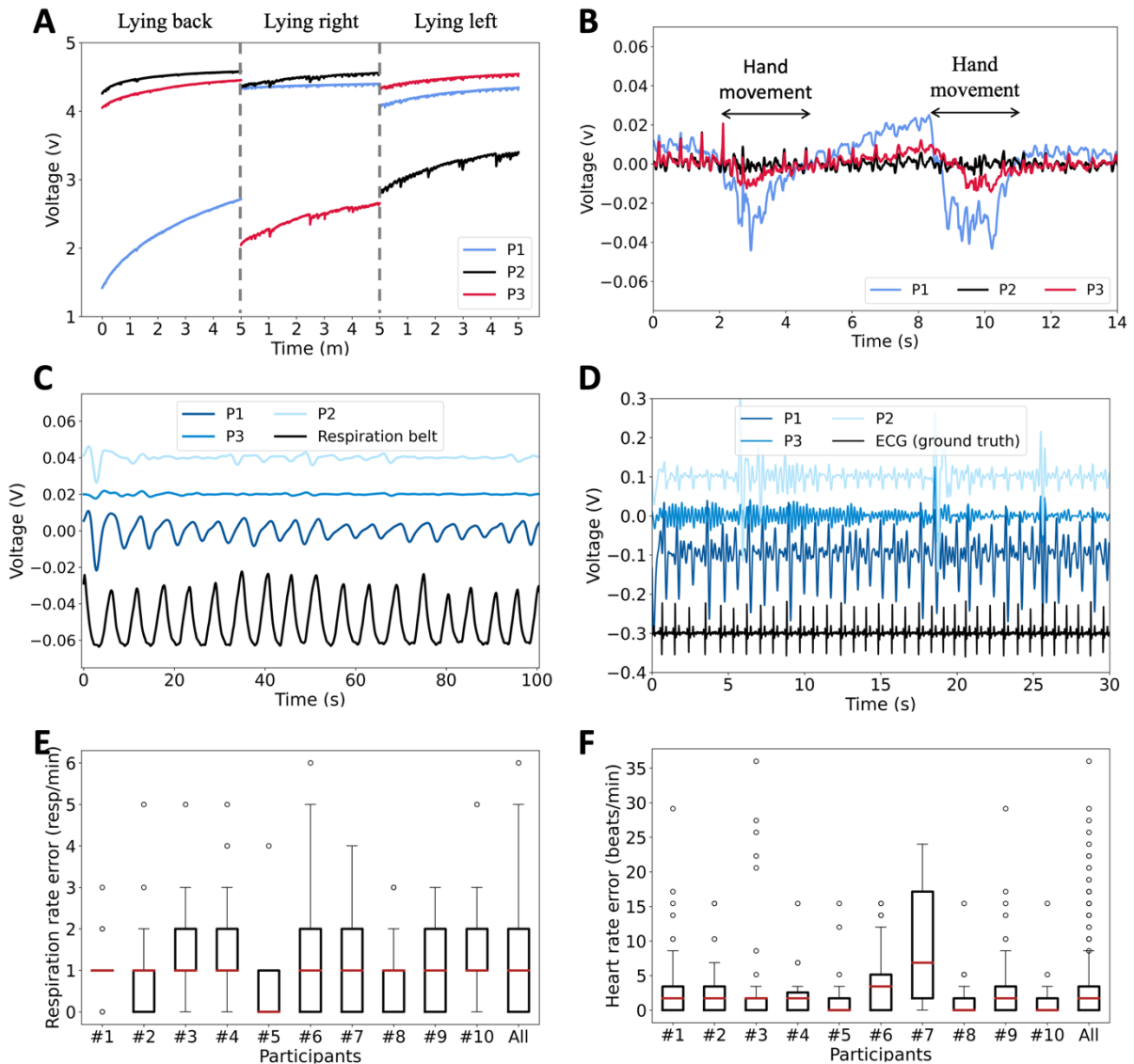


Fig. 3. Examples of time series signals of PhyMask pressure patches in sensing sleep posture, body movement, respiration, and cardiac signals, and results of PhyMask respiration and heart rate estimation. (A) Pressure patches baseline across three head postures. (B) DC-removed pressure patches baseline when the user is lying on their back and swinging their hand in time 2-4s and 9-11s. The periodic small spikes on the signals correspond to the heart beats. (C) The breathing signal along with the ground truth collected with the respiration belt. (D) The cardiac signal captured by the pressure patches along with the ECG ground truth. In both (C) and (D), the user is lying on their back, hence the back patch captures stronger cardiac and respiratory signals. (E) Performance of PhyMask in estimating breathing rate across all participants. (F) Performance of PhyMask in estimating heart rate across all participants.

Cardiac and respiration rate monitoring in different sleep postures

In this section, we validate PhyMask performance in robust measurement of physiological features for various users under different sleep posture settings. For this purpose, we asked 10 participants with various demographics to wear PhyMask and we recorded data in three sleep postures (lying on back, left, and right) each for 5 minutes. The details of the data collection and ground-truth labeling procedure can be found in Study design section. The full signal processing pipeline and our proposed algorithms for robust heart and breathing rate estimation are explained in PhyMask processing pipeline section.

Figure 3C illustrates the pressure sensors baseline can also be used to obtain respiration rate. In this example the participant is lying on their back and the respiratory-related head vibrations can clearly be seen in the pressed patch. Figure 3E shows the performance of PhyMask in estimating the breathing rate for all the participants across three sleep postures. The respiration metrics are very good, and the results demonstrate that PhyMask can measure respiration rate with a median error of about 1 resp/min.

PhyMask can also measure heart rate with very low error rates. An example of heartbeats signal collected from PhyMask pressure patches are depicted in Figure 3D. As can be seen in Figure 3F, the median heart rate error over all participants across all the sleep postures is about 1.7 beats/min, that is within the acceptable error margin (= 5 bpm) (37) for heart rate measurement (the results are separated for each sleep posture in Figure S4. The only participant with high error values is #7. Based on the ground truth signals, we find that this participant has weaker heartbeats that result in less perceptible head oscillations. We believe that in the future, we can further increase the sensitivity of our pressure patches in order to better detect these small movements. In the Discussion section, we share some of our thoughts on how we can achieve this.

Comfort of wear

At the end of our user study, we asked our participants to fill out a questionnaire regarding the PhyMask comfort and their preferences. The questions and the users' answers are presented in Figure S5. The results show that the majority found PhyMask quite comfortable. 9/10 users were interested in tracking their physiological signals during the sleep. None of the users had used sleep masks before, while 6/10 users had been using wearable tracking devices on a daily basis. While all the participants preferred PhyMask over PSG, only 3 participants preferred PhyMask over Fitbit/Oura, none of the whom owned any wearable tracking devices. An explanation for this can be that participants who already are used to wearing smart wearables, are also less willing to change their habit.

Discussion

In summary, we introduce a new all-textile system, the PhyMask, for monitoring a number of important sleep signals including EEG, EOG, respiration, heart rate, and gross body movement. Despite a plethora of commercial and research prototype sleep tracking solutions, we lack a reliable and comfortable solution that can continually monitor the whole range of sleep markers that are useful for clinical-grade sleep monitoring without impacting sleep. PhyMask bridges this gap and shows that all of these signals can be monitored by solely using soft textile-based sensors by leveraging a combination of soft hydrogel electrodes and sensitive textile-based pressure sensors. Such a system can be useful to enable high-quality clinical-grade sleep monitoring at home. Our results are very promising and demonstrate that we can measure a number of advanced sleep markers such as spindles and k-complexes in addition to sleep stages. We can also provide robust measures of physiological features from an unconventional place, i.e., head, with high accuracy across different sleep postures.

For the future work, one direction that we plan to explore, is improving sensitivity of the pressure sensor to very small amounts of pressure that is typical on the head. From the design and chemical structure point of view, there are three main factors that can be

altered to increase the sensitivity of the sensors to smaller applied pressures (1 kPa). First, changing the concentration of the siloxane molecules in the solution-phase functionalization process can lead to the change in the number of charge carriers -ions- in the system and, therefore, higher sensitivity. Second, the quality of fabric used in the active layer such as its weave density and the mesh size can play a major role in the performance of the sensor and the final number of layers used in the structure. The third factor that can improve the sensitivity of the sensor is the thickness and the weave density of the conductive fabric used as the top and bottom electrodes. These fabrics play a significant role in damping the pulses and it is anticipated that thinner fabrics can provide the capability of sensing weaker pulse pressures.

Our eventual objective is to enable the use of PhyMask in clinical-grade sleep monitoring at home to monitor sleep disorders. Our follow-on research will explore this direction further by performing more large-scale user studies with patients with different sleep disorders like sleep apnea and REM sleep disorder.

Materials and Methods

Fabrication of PhyMask

Figure 1B shows the PhyMask platform, which incorporates three biopotential electrodes and three pressure sensors. We made two biopotential electrodes with functional area of 1 cm x 1 cm and one electrode with functional area of 1 cm x 2 cm, serving as reference. We made the reference electrode slightly bigger to ensure better skin-electrode contact and hence more stable signal during long wear. For the pressure sensors, we made a large patch of functionalized ion-conductive layer, and then cut it into four 12 cm x 4 cm and two 6 cm x 4 cm sheets, each of which was sewn around the perimeter onto a sheet of silver fabric. Sewing together each pair of these joined gauze-silver sheets yielded three resistive sensors with a 4-layer structure. All six of these fabric electrodes are tightly sewn onto a commercially-available sleep mask – purchased from Amazon 4.5/5 with more than 4000 reviews, it was chosen because of its lightweight and adaptability to a wide variety of head shapes and sizes. For maximum comfort and to minimize the number of hard electronic components, we avoided using wires in our design. Instead, we used silver-plated nylon threads. In order to shield our wiring system from electromagnetic noises and make it laundering-stable, we cladded the silver threads with a three-layer fabric-based shield, comprising of polyurethane coated ripstop nylon cloth as the first layer, followed by a nanoscale (40–50 nm) coating of a hydrophobic polymer, PFDA as second, and encased within cotton piping as the last layer. Our wiring system serves as lightweight and flexible interconnects between the six sewn-on electrodes and the circuit board (PCB) microcontroller (MCU).

PhyMask board design

PhyMask uses a single low-power and compact circuit board for filtering, amplification, digitization, and transmission of the raw EEG, EOG, cardiac, and respiratory signals collected from the biopotential electrodes and the pressure patches. There are three main challenges in designing such a board: first, each of these signals has different characteristics that require specific electronics circuitry design; second, all of the signal channels need to be collected at high-enough sampling rate and transmitted at the same time to ensure real-time and accurate tracking; third, the board should have very low

power consumption enabling long-term usability of the system with a single battery charge. In the following, we explain the steps taken to tackle these challenges in the design of the PhyMask electronics.

As mentioned before, the board is connected to 3 biopotential electrodes (one reference and two sensors) and 3 pressure sensors. The biopotential electrodes provide the EOG and EEG signals while pressure sensors provide cardiorespiratory signals. Our board is composed of three main modules: 1) EEG and EOG signals acquisition, 2) cardiac and respiration signals acquisition, and 3) low-power wireless signal transmission. The board schematic is illustrated in Figure S7A.

Stage 1: EEG and EOG signals acquisition. EEG and EOG signals have very different characteristics. EOG signals, representing eye movements, have magnitudes in the orders of 100s of μV s with a frequency range of about DC-100Hz. EEG signals, however, are roughly three orders of magnitude weaker than the EOG signals and their frequency content during sleep can vary from 0.5Hz to about 30Hz. Examples of the EEG and EOG signals collected from PhyMask biopotential electrodes are depicted in Figure 2D and Figure S6, respectively.

To deal with this, we use two two-stage differential amplifiers each amplifying one biopotential signal with respect to the reference electrode. The gain of the first stage is about 30 and it outputs the EOG signal stream. We selected this level of amplification gain empirically such that the obtained EOG signal is clearly distinguishable, yet it does not saturate the next stage amplifier. This diminishes the need for a DC reject filter which consequently would have eliminated critical low-frequency contents of the EOG signal. In the second stage of the amplifier, we further amplify this signal by 2500 times and filter it to only pass through frequency content in the range of 1-50 Hz to acquire the EEG signal.

Stage 2: cardiac and respiration signals acquisition. As discussed earlier, the fabric-based pressure patches are designed to capture the subtle ballistics and head movements caused by cardiorespiratory activities. But these two signals are very different — the pressure response of respiration is stronger than the heartbeat, and the respiration signal contains very low frequency components (typically, below 1 Hz) whereas cardiac signal is in the 1-20 Hz frequency range. Examples of respiration and heartbeats signals collected from PhyMask pressure patches are depicted in Figure 3 (C and D), respectively.

The second stage of the board receives the signal from three pressure sensors and after using a voltage divider to translate resistance changes into changes in voltage, we use a voltage follower to create a copy of the signal with low output impedance for each channel, suitable for digitization. The resultant three signals represent the posture/respiration signals of the user. To find the heartbeat instances in these signals, we then DC reject and amplify the signals up to 400 times to find the ballistics of the veins covered by the sensor.

Stage 3: low-power wireless signal transmission. The last module of the board uses a low-power MCU with integrated BLE capability (nRF52811 (38)) to wirelessly transmit the acquired data to the host device. The MCU is capable of converting a maximum of 8 simultaneous analog channels into digital signals. This is less than the 10 analog channels captured by PhyMask, i.e., 2 EEG, 2 EOG, 3 cardiac, and 3 respiration. A naive solution would be to sequentially sample each channel and effectively reduce the sampling rate of all channels symmetrically. However, given the fact that the dominant frequency content of respiration is placed lower in frequency spectrum compared to other desired signals, we placed a 3:1 analog MUX to output one of the three respiration signals in each sampling

round. As a result, the effective sampling rate of the respiration signal is one-third of the other physiological signals. The decisions presented above result in sampling rate of 125 samples per second for EEG, EOG, and cardiac signals, while providing 42 samples per second for the respiration signal. These sampling rates are sufficient for reconstruction of the above signals given the fact that EEG, which contains the highest frequency content among all, requires a minimum sampling rate of 60 Hz to reach the Nyquist rate and the respiration signal requires a minimum sampling rate of 2 Hz.

Our choice of sampling rate is also limited by power consumption and hardware compatibility considerations. Higher sampling rate leads to higher transmission rate for the BLE module which greatly increases the power consumption; on the other hand, some host devices have lower bound restrictions for transmission interval in their BLE connection. In our setup, the transmission interval is set to 100 ms which makes the system capable of connecting with devices with more strict restrictions and leads to average power consumption of 3.3 mw. The power consumption of the analog processing components and the MUX is negligible in comparison with the MCU. This means that with a small battery of 250 mAh, 250/1.1 capacity, PhyMask can run up to 5 days. An image of the board, which has dimensions as small as 4 cm by 5 cm, is presented in Figure S7 (B and C).

Study design

In this section we explain the details of our user study and the ground truth labeling approach. All of these datasets were collected under Institutional Review Board approval. Our first data collection aims to evaluate PhyMask's ability in detecting heart rate, respiration, sleep posture, and gross body movement. For this, we asked 10 participants (average age of 27) to wear PhyMask and we recorded the output voltage in various stationary conditions. Participants varied in weight, 110-220 lb, and height, 5'1" to 6'. Four out of ten participants were females.

We asked our participants to lie down on their back, left, and right side, posing a sleep position that feels natural to them. We collected data for five minutes in each sleep posture. Then we demonstrated the participants a set of both smooth and jerky limb movements that are common during sleep (particularly for sleep disorders like periodic limb movement). We then repeated the first experiment and asked our participants to mimic these movements while in the sleep positions. The whole experiment led to a total of ~30 minutes of recording from each user. Each recording consists of ten channels, six of which correspond to pressure sensing patches and four corresponding to the biopotential fabric electrodes.

To assess the PhyMask's performance, we collect ground truth measures of the target physiological signals. For heart rate, we use a three-channel ECG measurement (2 wrists and an ankle) using the AD8232 evaluation board (39) (sampling rate of 200 Hz), and for respiration, we used a Go Direct respiration belt (40) (sampling rate of 10 Hz).

Our second data collection aims to validate PhyMask's ability in measuring the brain waves (EEG) in a more uncontrolled and naturalistic setting and to evaluate biopotential signal quality over a long time of wear. For this, we asked a participant (Male, weight = 160lbs) to wear PhyMask for five nights during sleep and we collected the signals for total of 2118 minutes (about 7 hours per night). Due to the COVID-19 precaution, the experiment took place in participant's home, providing him a safe environment to perform the study. In addition, it allowed us to collect more naturalistic sleep behavior.

To evaluate how PhyMask compares to commercially-available sleep tracking wearables, we asked our participant to wear a Fitbit Charge 2 and an Oura Ring (fit size 11) on the non-dominant hand. The Fitbit and Oura Ring are the dominant sleep tracking wearables in the market, and this comparison allows us to gauge the benefits that PhyMask can provide due to measuring the EEG signal in addition to the physiological signals collected by these wearables.

For ground truth, the PSG data was collected simultaneously with data from PhyMask. PSG included electroencephalographic (EEG: Fp1, Fp2, Cz, O1, O2), chin electromyographic (EMG), and electrooculographic (EOG) recordings performed according to American Academy of Sleep Medicine (AASM) rules (41) (the electrodes placement is shown in Figure S8). The electroconductive paste (Ten20 (42)) were used to improve contact between the participant's scalp and the gold cup electrodes (with 10 mm diameter (43)). The eight channels of data were collected via an OpenBCI Cyton amplifier (44). In order to synchronize PhyMask's EEG signals with the PSG setup, the two PhyMask's EEG channels were also collected via the OpenBCI Cyton amplifier through the expansion Daisy Module (44). The OpenBCI board was wirelessly connected to a laptop by the USB Dongle. The raw EEG signals were sampled at a rate of 125Hz, passed through a 60Hz notch filter, a 0.5-50Hz bandpass filter, and finally processed through the use of a mean smoothing filter to mitigate movement artifacts. Figure 4A shows a user sleeping while wearing PhyMask, sleep tracking wearables, and all the ground truth devices.

Sleep stages (Wake, N1, N2, N3, REM sleep) were scored in 30-sec epochs by certified sleep experts according to sleep scoring guideline of AASM (45), separately for both PSG and PhyMask. In addition, the sleep micro-events i.e., spindles and k-complexes, were annotated for one night data (408 number of spindles and 235 number of K-complexes). For this, a sleep specialist first marked the events with Embla RemLogic PSG software (46), and then visually validated all the events.

PhyMask processing pipeline

Sleep spindle and k-complex detection. Sleep spindles are brief bursts of neural oscillations (9–16Hz, 0.5–3s) generated by the interplay of the thalamic reticular nucleus and other thalamic nuclei during NREM sleep (N2 and N3 stages) (shown in Figure 2D). Like spindle, k-complex is a great hallmark of NREM sleep stage 2 and is often followed by a sleep spindle. K-complexes are generated in widespread cortical locations though they tend to predominate over the frontal parts of the brain. K-complex characteristics are very different from spindles. They consist of a brief negative sharp wave immediately followed by a positive component, creating slow-wave (0.8 Hz) and delta (1.6–4.0 Hz) oscillations of 0.5–3s in duration. We train two different models of the same architecture for detection of spindles and k-complexes. Several classification algorithms were tested during this study, including random forests, neural networks, and support vector machines. We found the random forest classifier to provide the best performance.

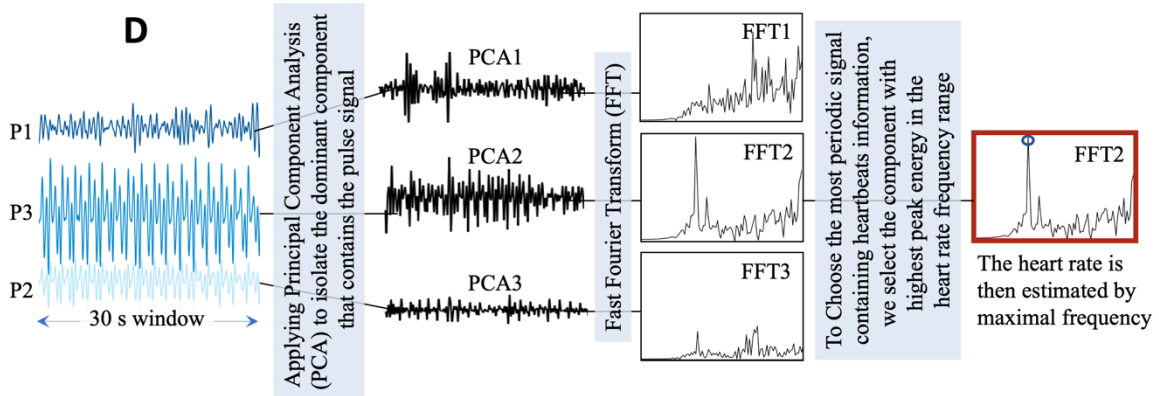
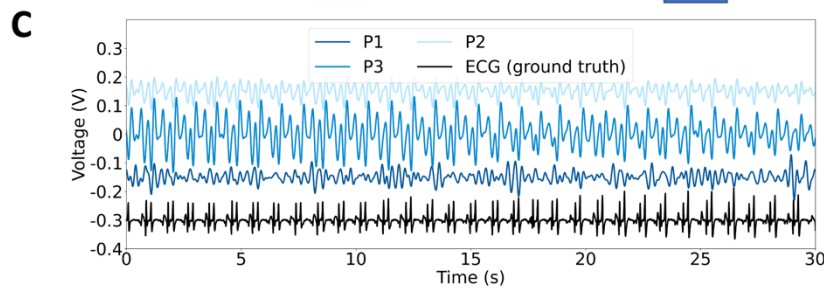
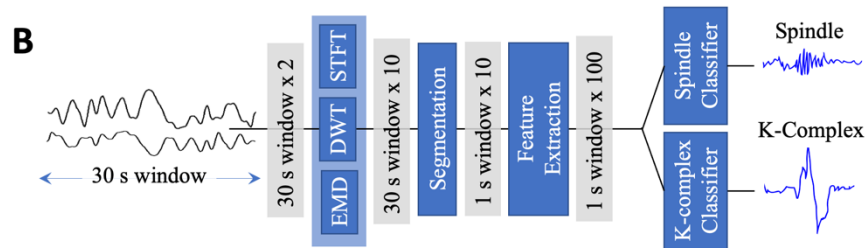
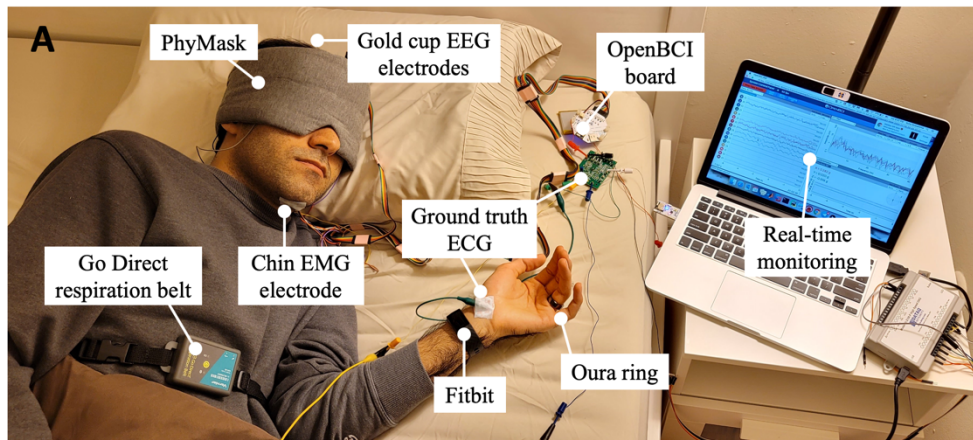


Fig. 4. Image of the user study setup and schematic of PhyMask processing pipeline. (A) Data collection setup. (B) PhyMask spindle and k-complex detection algorithm pipeline. (C) Time series of the PhyMask pressure patches signals along with ECG ground truth. While the user is lying on their back, the side patches capture the pulses stronger than the back patch. (D) PhyMask heart rate detection algorithm pipeline.

In order to prepare the data for our binary random forest classifier, we first apply a 5th order Butterworth filter with a passband of 0.5-35Hz to filter out noises from the EEG streams. Then, we extract features in both time and frequency domains. Our feature extraction pipeline is summarized in Figure 4B. In the first stage, we derive Short-time Fourier Transform (STFT), Discrete Wavelet Transform (DWT), and Empirical Mode Decomposition (EMD) features from 30-second epochs of the EEG streams and append

them as additional channels to the original raw signal. In the second stage, we extract statistical features from overlapping windows of the output signal of the first stage. We empirically choose a window size of 1s (125 samples) for both spindle and k-complex detection. The details of feature extraction pipeline can be found in Supplementary Materials.

Respiration and heart rate estimation. In order to accurately estimate respiratory rate from the pressure sensors baseline signals, we first apply FFT to find the frequency bin with the highest power resulted from the respiration signal. Then, we perform band-pass filtering based around the FFT peak to avoid counting fluctuations of the second harmonic. We then count the number of peaks in one-minute-long windows of the filtered time series to obtain the respiration rate. The estimated respiration rate is updated once every half-minute (the step size is 30s). The strongest respiration signal is obtained from the patch on which the head is resting, i.e. the most pressure is sensed on.

The estimation of the heart rate is more challenging as the cardiac signal captured by the pressure patches has very a low SNR due to the mixed-in involuntary head movements, and the noise in all frequency bins. Furthermore, the amplitude of the cardiac signal can also be affected by many factors including sleep posture and user's physiological characteristics.

Generally, the signal captured by the patch under pressure in each sleep posture has better resolution in capturing the small head movements related to cardiac activity. An example is shown in Figure 3D, where the user is lying on their back and the back patch (P1) can clearly capture the heartbeats, better than the other two sensors. However, this assumption does not always hold true. Figure 4C shows another example of when the user is lying on their back and this time, the back pressure signal (P1) is quite corrupted while the right (P3) and left (P2) signals clearly detect the heartbeats. This can happen due to several reasons. Having wrinkles in the pressed patch decreases the sensor sensitivity and results in poor and noisy signal. Also, for the users who naturally have strong superficial temporal artery pulse on the temple, the heartbeat signals captured from side patches are much stronger than the back patch that only detects the subtle head motion caused by the Newtonian reaction to the influx of blood at each beat. Therefore, we have two main challenges that we need to encounter when designing our algorithm: (1) the heartbeat signal is weak and usually interfered by many sources of noises, and (2) the signal quality of patches differs across different users and sleep postures. In the following, we describe our proposed heart rate detection algorithm summarized in Figure 4D.

In order to block the DC baseline, respiration related frequency components, and higher frequency noises, we apply a 5th order butterworth filter with a passband of 0.75-3Hz on three cardiac signals. Please note that a normal adult's resting pulse rate falls within [0.75, 2] Hz, or [45, 120] beats/min. After eliminating some of the noise, we need to isolate the heartbeat component of the three signals. In order to do this, we use Principal Component Analysis (PCA) to isolate the dominant component that contains the pulse signal. We consider each pressure patch signal stream as a separate data point and use PCA to find a set of basis vectors along which the signal has the most variation (the mathematical computation is included in Supplementary Materials). We then select the most periodic component for heart rate estimation, where the periodicity of the input signal is calculated as the percentage of the spectral power accounted for by the frequency with maximal power to the total spectral power. The heart rate is then estimated as $\frac{60}{f_{pulse}}$ beats/min,

where f_{pulse} is the maximal frequency of the selected component. Please note that we perform PCA on a 30-second window and slide it with a hop size of 10s.

References

1. CDC - Sleep and Chronic Disease - Sleep and Sleep Disorders, (available at https://www.cdc.gov/sleep/about_sleep/chronic_disease.html).
2. B. M. Altevogt, H. R. Colten, others, *Sleep disorders and sleep deprivation: an unmet public health problem* (National Academies Press, 2006).
3. Z. Jia, A. Bonde, S. Li, C. Xu, J. Wang, Y. Zhang, R. E. Howard, P. Zhang, in *Proceedings of the 15th ACM Conference on Embedded Network Sensor Systems* (Association for Computing Machinery, New York, NY, USA, 2017; <https://doi.org/10.1145/3131672.3131679>), *SenSys '17*.
4. T. Rahman, A. T. Adams, R. V. Ravichandran, M. Zhang, S. N. Patel, J. A. Kientz, T. Choudhury, in *Proceedings of the 2015 ACM International Joint Conference on Pervasive and Ubiquitous Computing* (Association for Computing Machinery, New York, NY, USA, 2015; <https://doi.org/10.1145/2750858.2804280>), *UbiComp '15*, pp. 39–50.
5. J. Liu, Y. Wang, Y. Chen, J. Yang, X. Chen, J. Cheng, in *Proceedings of the 16th ACM International Symposium on Mobile Ad Hoc Networking and Computing* (2015), pp. 267–276.
6. M. H. Li, A. Yadollahi, B. Taati, Noncontact vision-based cardiopulmonary monitoring in different sleeping positions. *IEEE J. Biomed. Heal. informatics.* **21**, 1367–1375 (2016).
7. Fitbit Official Site for Activity Trackers & More, (available at <https://www.fitbit.com/global/us/home>).
8. Garmin vivofit® 4 | Fitness Activity Tracker, (available at <https://buy.garmin.com/en-US/US/p/582444>).
9. Actiwatch Spectrum Activity monitor | Philips Healthcare, (available at <https://www.usa.philips.com/healthcare/product/HC1046964/actiwatch-spectrum-activity-monitor>).
10. WHOOP - The World's Most Powerful Fitness Membership., (available at <https://www.whoop.com/>).
11. Oura Ring: Accurate Health Information Accessible to Everyone, (available at <https://ouraring.com/>).
12. K. Meng, S. Zhao, Y. Zhou, Y. Wu, S. Zhang, Q. He, X. Wang, Z. Zhou, W. Fan, X. Tan, J. Yang, J. Chen, A Wireless Textile-Based Sensor System for Self-Powered Personalized Health Care. *Matter.* **2**, 896–907 (2020).
13. A. Kiaghadi, S. Z. Homayounfar, J. Gummesson, T. Andrew, D. Ganesan, Phyjama: Physiological Sensing via Fiber-Enhanced Pyjamas. *Proc. ACM Interact. Mob. Wearable Ubiquitous Technol.* **3** (2019), doi:10.1145/3351247.
14. F. Moreno-Pino, A. Porras-Segovia, P. López-Esteban, A. Artés, E. Baca-García, Validation of Fitbit charge 2 and Fitbit Alta HR against polysomnography for assessing sleep in adults with obstructive sleep apnea. *J. Clin. Sleep Med.* **15**, 1645–1653 (2019).
15. D. J. Miller, M. Lastella, A. T. Scanlan, C. Bellenger, S. L. Halson, G. D. Roach, C. Sargent, A validation study of the WHOOP strap against polysomnography to assess sleep. *J. Sports Sci.* **38**, 2631–2636 (2020).
16. Muse™ - Meditation Made Easy with the Muse Headband, (available at <https://choosemuse.com/>).
17. Dreem 2 - Sleep, finally., (available at <https://dreem.com/>).
18. Wearable EEG headband “BrainBit”, (available at <https://brainbit.com/>).

19. SmartSleep Deep Sleep Headband | Philips, (available at <https://www.usa.philips.com/c-e/smartsleep/deep-sleep-headband.html>).
20. S. Rostamina, A. Lamson, S. Maji, T. Rahman, D. Ganesan, W!NCE: Unobtrusive Sensing of Upper Facial Action Units with EOG-Based Eyewear. *Proc. ACM Interact. Mob. Wearable Ubiquitous Technol.* **3** (2019), doi:10.1145/3314410.
21. S. Z. Homayounfar, S. Rostamina, A. Kiaghadi, X. Chen, E. T. Alexander, D. Ganesan, T. L. Andrew, Multimodal Smart Eyewear for Longitudinal Eye Movement Tracking. *Matter.* **3**, 1275–1293 (2020).
22. S. Z. Homayounfar, A. Kiaghadi, D. Ganesan, T. L. Andrew, {PressION}: An All-Fabric Piezoionic Pressure Sensor for Extracting Physiological Metrics in Both Static and Dynamic Contexts. *J. Electrochem. Soc.* **168**, 17515 (2021).
23. N. Hennies, M. A. L. Ralph, M. Kempkes, J. N. Cousins, P. A. Lewis, Sleep spindle density predicts the effect of prior knowledge on memory consolidation. *J. Neurosci.* **36**, 3799–3810 (2016).
24. A. Jegou, M. Schabus, O. Gosseries, B. Dahmen, G. Albouy, M. Desseilles, V. Sterpenich, C. Phillips, P. Maquet, C. Grova, others, Cortical reactivations during sleep spindles following declarative learning. *Neuroimage.* **195**, 104–112 (2019).
25. K. Kam, A. Parekh, R. A. Sharma, A. Andrade, M. Lewin, B. Castillo, O. M. Bubu, N. J. Chua, M. D. Miller, A. E. Mullins, others, Sleep oscillation-specific associations with Alzheimer’s disease CSF biomarkers: novel roles for sleep spindles and tau. *Mol. Neurodegener.* **14**, 10 (2019).
26. J. El Helou, V. Navarro, C. Depienne, E. Fedirko, E. LeGuern, M. Baulac, I. An-Gourfinkel, C. Adam, K-complex-induced seizures in autosomal dominant nocturnal frontal lobe epilepsy. *Clin. Neurophysiol.* **119**, 2201–2204 (2008).
27. A. Roebuck, V. Monasterio, E. Geder, M. Osipov, J. Behar, A. Malhotra, T. Penzel, G. D. Clifford, A review of signals used in sleep analysis. *Physiol. Meas.* **35**, R1 (2013).
28. J. N. Acharya, A. J. Hani, J. Cheek, P. Thirumala, T. N. Tsuchida, American Clinical Neurophysiology Society guideline 2: guidelines for standard electrode position nomenclature. *Neurodiagn. J.* **56**, 245–252 (2016).
29. G. Balakrishnan, F. Durand, J. Guttag, in *2013 IEEE Conference on Computer Vision and Pattern Recognition* (2013), pp. 3430–3437.
30. R. W. Thatcher, Coherence, Phase Differences, Phase Shift, and Phase Lock in EEG/ERP Analyses. *Dev. Neuropsychol.* **37**, 476–496 (2012).
31. A. H. Ghaderi, S. Moradkhani, A. Haghightafard, F. Akrami, Z. Khayyer, F. Balçı, Time estimation and beta segregation: An EEG study and graph theoretical approach. *PLoS One.* **13**, e0195380 (2018).
32. R. Ranjan, R. Arya, S. L. Fernandes, E. Sravya, V. Jain, A fuzzy neural network approach for automatic K-complex detection in sleep EEG signal. *Pattern Recognit. Lett.* **115**, 74–83 (2018).
33. S. V Schönwald, L. Emerson, R. Rossatto, M. L. F. Chaves, G. J. L. Gerhardt, Benchmarking matching pursuit to find sleep spindles. *J. Neurosci. Methods.* **156**, 314–321 (2006).
34. M. de Zambotti, L. Rosas, I. M. Colrain, F. C. Baker, The Sleep of the Ring: Comparison of the ÖURA Sleep Tracker Against Polysomnography. *Behav. Sleep Med.* **17**, 124–136 (2019).
35. M. de Zambotti, A. Goldstone, S. Claudatos, I. M. Colrain, F. C. Baker, A validation study of Fitbit Charge 2™ compared with polysomnography in adults. *Chronobiol. Int.* **35**, 465–476 (2018).
36. M. J. L. Ravesloot, J. P. Van Maanen, L. Dun, N. De Vries, The undervalued potential of positional therapy in position-dependent snoring and obstructive sleep apnea? a review of

- the literature. *Sleep Breath*. **17**, 39–49 (2013).
37. M. A. Hassan, A. S. Malik, D. Fofi, N. Saad, B. Karasfi, Y. S. Ali, F. Meriaudeau, Heart rate estimation using facial video: A review. *Biomed. Signal Process. Control*. **38**, 346–360 (2017).
 38. nRF52811 - Bluetooth 5.2 SoC - nordicsemi.com, (available at <https://www.nordicsemi.com/Products/Low-power-short-range-wireless/nRF52811>).
 39. AD8232 Datasheet and Product Info | Analog Devices, (available at <https://www.analog.com/en/products/ad8232.html>).
 40. Go Direct® Respiration Belt - Vernier, (available at <https://www.vernier.com/product/go-direct-respiration-belt/>).
 41. Practice Standards - American Academy of Sleep Medicine – Association for Sleep Clinicians and Researchers, (available at <https://aasm.org/clinical-resources/practice-standards/>).
 42. Ten20 EEG Conductive Paste - 8oz Jars - 3 pack, (available at <https://bio-medical.com/ten20-eeg-conductive-paste8oz-jars-3-pack.html>).
 43. Gold Cup Electrodes – OpenBCI Online Store, (available at <https://shop.openbci.com/products/openbci-gold-cup-electrodes?variant=37345591591070>).
 44. Cyton + Daisy Biosensing Boards (16-Channels) – OpenBCI Online Store, (available at <https://shop.openbci.com/collections/frontpage/products/cyton-daisy-biosensing-boards-16-channel?variant=38959256526>).
 45. R. B. Berry, R. Brooks, C. E. Gamaldo, S. M. Harding, C. Marcus, B. V Vaughn, others, The AASM manual for the scoring of sleep and associated events. *Rules, Terminol. Tech. Specif. Darien, Illinois, Am. Acad. Sleep Med.* **176**, 2012 (2012).
 46. Embla RemLogic PSG Software | Natus, (available at <https://neuro.natus.com/products-services/embla-remlogic-software>).
 47. C. Yücelbağcı, S. Sule Yücelbağcı, S. Özgenç, G. Tezel, S. Küçüktürk, N. Sebnem Yosunkaya, Automatic detection of sleep spindles with the use of STFT, EMD and DWT methods. *Neural Comput. Appl.* **29**, 17–33 (2018).
 48. J. Costa, M. Ortigueira, A. Batista, T. Paiva, An Automatic Sleep Spindle detector based on WT, STFT and WMSD. *Int. J. Biomed. Biol. Eng.* **6**, 397–400 (2012).
 49. M. J. Shensa, The discrete wavelet transform: wedding the a trous and Mallat algorithms. *IEEE Trans. signal Process.* **40**, 2464–2482 (1992).
 50. N. E. Huang, Z. Shen, S. R. Long, M. C. Wu, H. H. Shih, Q. Zheng, N.-C. Yen, C. C. Tung, H. H. Liu, The empirical mode decomposition and the Hilbert spectrum for nonlinear and non-stationary time series analysis. *Proc. R. Soc. London. Ser. A Math. Phys. Eng. Sci.* **454**, 903–995 (1998).
 51. N. V Chawla, K. W. Bowyer, L. O. Hall, W. P. Kegelmeyer, SMOTE: synthetic minority over-sampling technique. *J. Artif. Intell. Res.* **16**, 321–357 (2002).

Acknowledgments

This work was funded by the National Science Foundation under agreement CSR Medium 1763524. S.R. and D. G. acknowledge support from the National Science Foundation under agreements 1815347 and 1839999. S.Z.H. and T.L.A. also thank the David and Lucile Packard Foundation for providing partial support.

Supplementary Materials for

PhyMask: Robust Sensing of Brain Activity and Physiological Signals During Sleep with an All-textile Eye Mask

Soha Rostaminia, S. Zohreh Homayounfar, Ali Kiaghadi, Trisha L. Andrew, Deepak Ganesan

This PDF file includes:

Supplementary Text
Figs. S1 to S8

Supplementary Text

Sensitivity and specificity definitions

$$\text{Sensitivity} = \frac{TP}{TP + FN} \qquad \text{Specificity} = \frac{TN}{TN + FP} \qquad (\text{S3})$$

Accuracy, precision, recall, and F1 score definitions

$$\begin{aligned} \text{Accuracy} &= \frac{TP + TN}{TP + TN + FP + FN} & \text{Precision} &= \frac{TP}{TP + FP} \\ \text{Recall} &= \frac{TP}{TP + FN} & \text{F1 score} &= \frac{2TP}{2TP + FP + FN} \end{aligned} \qquad (\text{S4})$$

where TP (true positive) is the number of actual positive epochs which are correctly classified; TN (true negative) is the number of actual negative epochs which are correctly classified; FP (false positive) is the number of actual negative epochs which are incorrectly classified as positive; FN (false negative) is the number of actual positive epochs which are incorrectly classified as negative.

Sleep Spindle and K-complex feature extraction pipeline

After filtering out the EEG streams, we chunk them into 30-second epochs and then apply time-space analysis methods to capture both frequency and location information.

Short-time Fourier transform (STFT). One of the methods used is Short-time Fourier transform (STFT). STFT is used to derive the frequency and phase content for sections of the EEG signal. In the literature, STFT is widely used as one of the main features for automatic spindle and k-complex detection (47, 48). STFT computation algorithm divides the input vector into overlapping shorter segments of equal length and then Fourier transform is computed separately on each segment. The output is a 3-dimensional time-series containing information regarding the frequency content of each time segment. Given the different frequency characteristic of spindle and k-complex, we extract two separate features from STFT for each event.

For spindle that has a frequency content of 9–16Hz, we extract 1) sum of the powers of frequency components of the signal in 10–12 Hz, and 2) sum of the powers of frequency components of the signal within 9–16 Hz of the signal. For k-complex, which has most of its frequency content around 0.8 Hz and within 1.6-4.0 Hz, we extract 1) sum of the powers of frequency components of the signal within 0.5–1 Hz, and 2) sum of the powers of frequency components of the signal within 1.5–4.5 Hz. We then up-sample the outputs to generate a time-series of the same length as the original EEG signal and augment them with the raw EEG stream as additional channels.

Discrete Wavelet transform (DWT). To further investigate the frequency content of the EEG time-series data, we use Discrete Wavelet transform (DWT) (49). DWT obtains low-frequency resolution and high-frequency information using long- and short-time windows, respectively. Because of this, DWT is appropriate for the analysis of the non-stationary signals such as EEG (47). 2-level DWT and Daubechies-2 (db2) mother wavelet is used in

our computation, and the second-level coefficients are taken as the output. The output is up-sampled and appended to the raw EEG and extracted STFT features.

Empirical Mode Decomposition (EMD). Empirical mode decomposition (EMD) can be used for nonlinear and non-stationary signals such as EEG (50). In this method, a signal is divided into substatements referred to as intrinsic mode functions (IMF) and subpiece (residue). The main idea behind EMD is to locally reconstruct a signal. The reconstruction is a sum of a local trend and detail. The local trend implies the low-frequency components of the signal (residual), while the local detail (IMF) is the high-frequency parts. According to this method, a signal is recursively separated step by step. Then a certain number of IMFs and residuals are obtained depending on the content of the signal. We choose the first IMF component as the output, and then append it to the output of the previous step. Yücelbaç et al. (47) has also utilized EMD for automatic spindle detection. In their solution, they apply binary thresholding on the first IMF component derived from the EMD of a single EEG stream to detect spindle events.

Statistical feature extraction. In this step, we chunk the output of the previous step, i.e., a multi-channel signal consisting of the raw EEG, extracted STFT features, DWT features, and the EMD components, into overlapping 1-second windows and then extract statistical features including maximum, mean, median, standard deviation, sum, energy, mean-crossing, interquartile range, 10th percentile, and 90th percentile. Finally in order to train our random forest classifier, we use SMOTE (51) to balance the training dataset.

Mathematical computation for heart rate calculation

The 3 filtered pressure patch signals at time t are represented by $m_t = [y_1(t), y_2(t), y_3(t)]$. PCA finds the principal axes of variation of the signal as the eigenvectors of the covariance matrix of the data $\sum m_t$, i.e.

$$\sum m_t \Phi m_t = \Phi \Lambda m_t \quad (S5)$$

where Λm_t denotes a diagonal matrix of the eigenvalues λ_1, λ_2 , and λ_3 corresponding to the eigenvectors in the columns of Φm_t , ϕ_1, ϕ_2 , and ϕ_3 . We finally obtain three 1-D signals $s_i(t)$ by projecting m_t onto ϕ_i .

$$s_i(t) = \sum_t m_t \phi_i \quad (S6)$$

We then select the most periodic components $p(t) = \text{argmax}_{s_i} h(s_i(t))$ for heart rate estimation, where the function $h(\cdot)$ calculates the periodicity of the input signal as the percentage of the spectral power accounted for by the frequency with maximal power to the total spectral power. The heart rate is then estimated as $\frac{60}{f_{pulse}}$ beats/min, where f_{pulse} is the maximal frequency of $s_p(t)$.

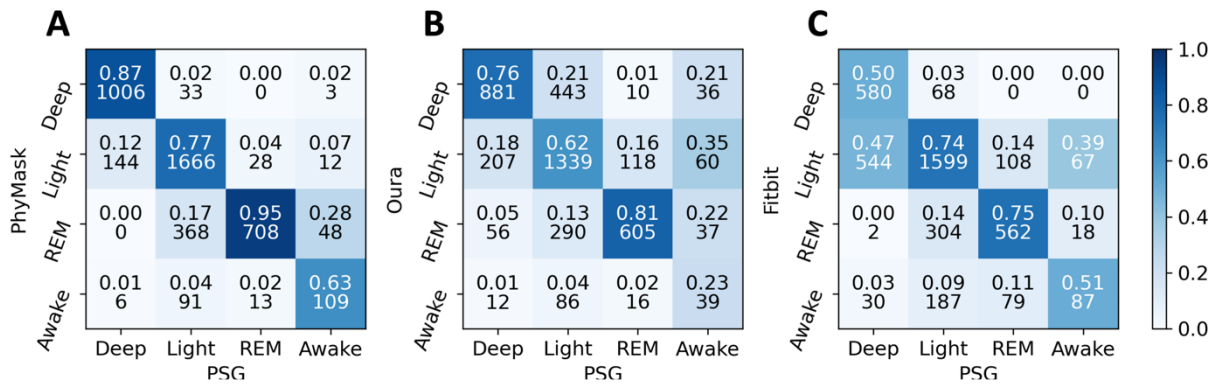


Fig. S1.

Comparison of the PhyMask with Oura and Fitbit in sleep stage classification.

Confusion matrices for (A) PhyMask, (B) Oura, and (C) Fitbit are plotted for classifying four different sleep stages including deep, light, REM, and awake. The results are computed against PSG sleep tracking approach as the ground truth.

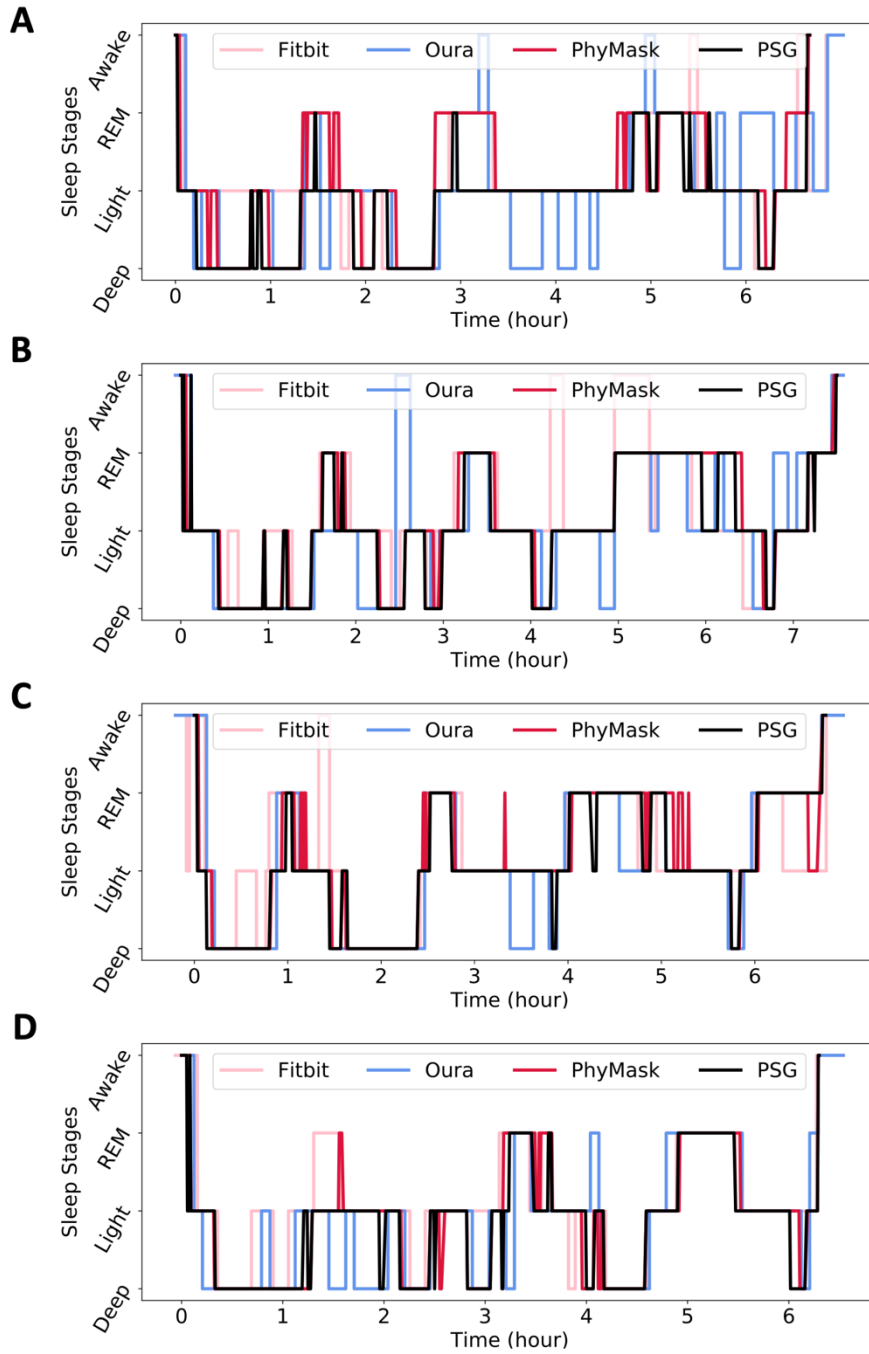


Fig. S2.

Time series of extracted sleep stages from PhyMask, Oura, Fitbit, and the ground truth (PSG). The extracted sleep stages of four nights for ground-truth (PSG), PhyMask, Oura, and Fitbit are illustrated for comparison.

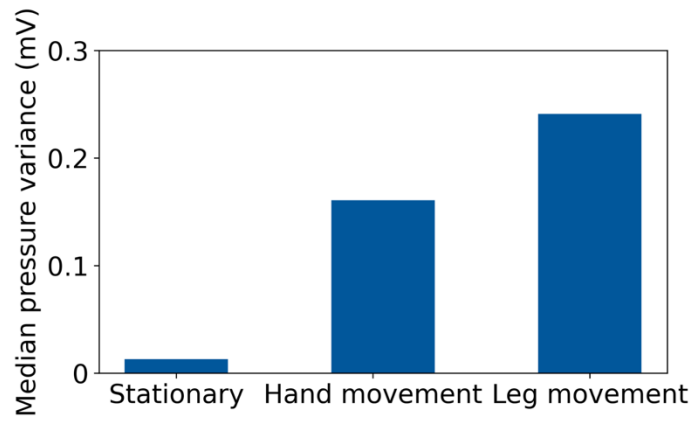


Fig. S3.

Comparing pressure sensors voltage changes in different gross body movement scenarios. The median variance of baseline signal voltage of the pressure patches for stationary, hand movement, and leg movement scenarios are depicted across all sleep postures and participants.

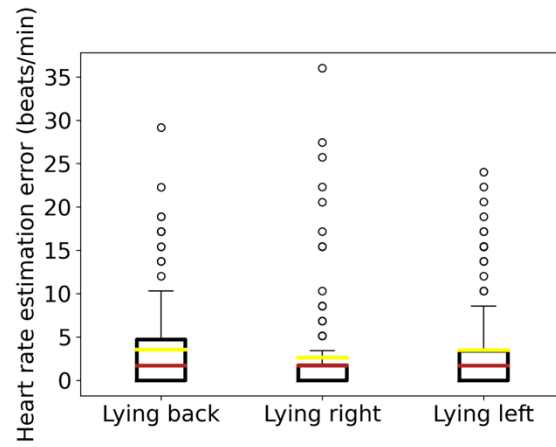


Fig. S4.
Performance of PhyMask in estimating heart rate in different sleep postures across all participants.

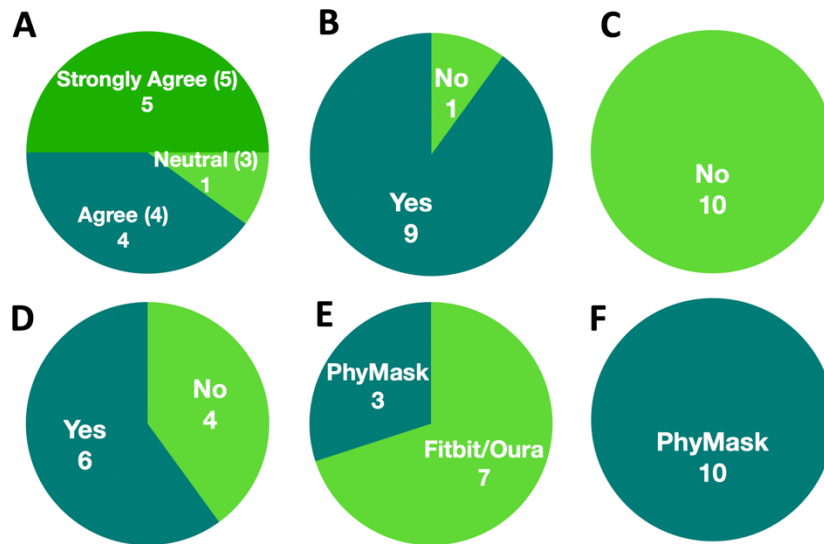


Fig. S5.

Summary of subjective assessment report. The questions asked are as follows, (A) Is PhyMask comfortable? (B) Are you interested in tracking your vital signs during sleep? (C) Do you usually use sleep masks? (D) Do you usually use Fitbit/Oura? (E) PhyMask or Fitbit/Oura? (F) PhyMask or PSG?

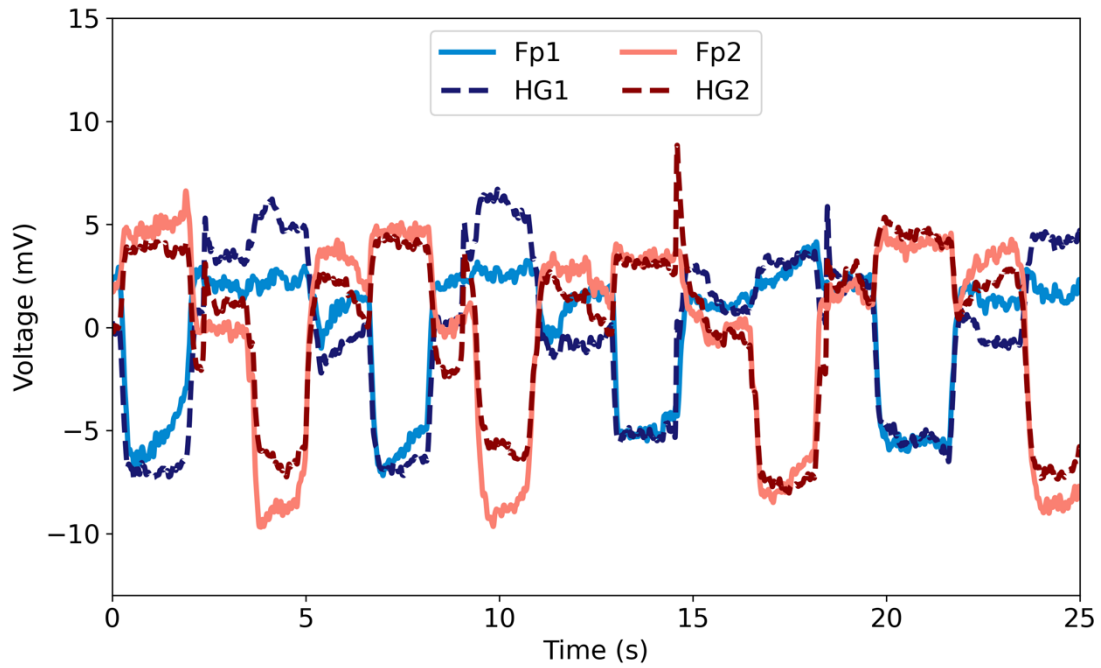


Fig. S6.
Time series of the EOG signal collected from hydrogel and standard 3M electrodes. During data collection, the participant was lying on their back and looking right and left periodically with closed eyes.

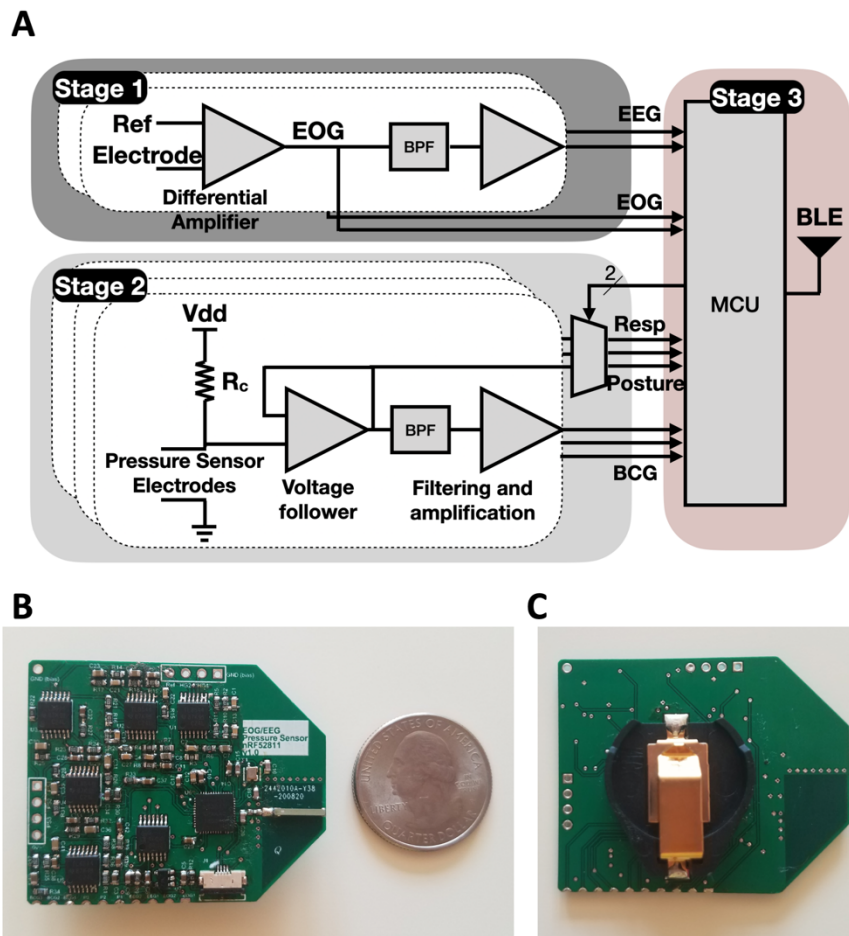


Fig. S7.

PhyMask board. (A) Block diagram of analog circuit board. The board has three main stages responsible for biopotential signals sensing, pressure sensors sensing, and signals transmission. (B) Front view of the board, comparing its dimension with a quarter dollar coin. (C) Rear view of the board, where the battery should be placed.

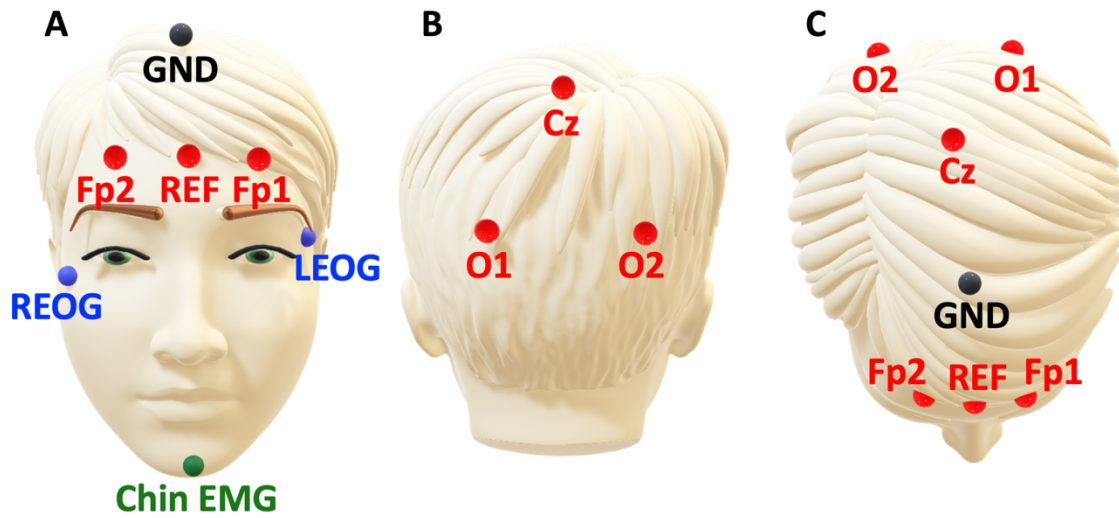


Fig. S8.
The ground truth gold-cup electrodes' placements used in our sleep monitoring study, based on the standard 10-20 EEG recording system.